

Ground-state phase structure of the spin- $\frac{1}{2}$ anisotropic planar pyrochlore

P H Y Li and R F Bishop

School of Physics and Astronomy, Schuster Building, The University of Manchester, Manchester, M13 9PL, UK

Abstract. We study the zero-temperature ground-state (GS) properties of the spin- $\frac{1}{2}$ anisotropic planar pyrochlore, using the coupled cluster method (CCM) implemented to high orders of approximation. The system comprises a J_1 - J_2 model on the checkerboard lattice, with isotropic Heisenberg interactions of strength J_1 between all nearest-neighbour pairs of spins on the square lattice, and of strength J_2 between half of the next-nearest-neighbour pairs (in the checkerboard pattern). We calculate results for the GS energy and average local GS on-site magnetization, using various antiferromagnetic classical ground states as CCM model states. We also give results for the susceptibility of one of these states against the formation of crossed-dimer valence-bond crystalline (CDVBC) ordering. The complete GS phase diagram is presented for arbitrary values of the frustration parameter $\kappa \equiv J_2/J_1$, and when each of the exchange couplings can take either sign.

PACS numbers: 75.10.Jm, 75.30.Kz, 75.10.Kt, 75.50.Ee

1. Introduction

The study of frustrated quantum spin systems, both theoretically and experimentally, has become a field of intense activity in recent years, especially in the context of quantum phase transitions [1–3]. In particular, the experimental investigation of a wide variety of quasi-two-dimensional materials with fascinating properties has progressed hand-in-hand with the theoretical study of spin-lattice models believed to capture their most important behaviour. The interplay between frustration, both geometrical and dynamical, and quantum fluctuations can produce interesting zero-temperature ($T = 0$) ground-state (GS) quantum phase transitions. These can involve phases ranging from ones with quasiclassical magnetic long-range order (LRO), such as Néel antiferromagnetic (AFM) order, to others such as valence-bond solids and spin liquids, which have no classical counterparts. The stable GS phases are strongly influenced by parameters such as the spin quantum number s of the magnetically active ions situated on the sites of the lattice, the dimensionality, the coordination number (z), and geometry of the lattice, the number of magnetic bonds and whether they are ferromagnetic (FM) or AFM in nature.

One of the key motivators that has spurred continued interest in highly frustrated quantum spin-lattice systems, has been the possibility of finding situations where a novel phase with no classical counterpart forms the stable GS phase. In particular, the search for quantum spin-liquid phases has received intense interest, ever since they were first proposed by Anderson [4] over 40 years ago. Even though we now know that the example proposed by Anderson, namely, the GS phase of a spin-1/2 Heisenberg antiferromagnet (HAFM) on a triangular lattice (i.e., with spins interacting via nearest-neighbour (NN) isotropic Heisenberg AFM exchange interactions only), is not a spin liquid, the search for such states continues in other systems. It is widely believed that prime candidates in this context are those which at the classical ($s \rightarrow \infty$) level display a GS phase in some region of their phase diagram that has macroscopic degeneracy. In particular, much attention has thereby focused on frustrated quantum spin systems that are built from tetrahedra coupled into two-dimensional (2D) or three-dimensional (3D) lattice networks [5–26].

The pyrochlore lattice comprises a 3D arrangement of corner-sharing tetrahedra, and it is well known that essentially all compounds that crystallize into the pyrochlore structure display unusual magnetic properties. In order to simplify the study of the 3D pyrochlore, but without losing any of its magnetic frustration, it is also common to project the 3D vertex-sharing lattice of tetrahedra onto a 2D plane. Each tetrahedron has four spins at its vertices, with each of its six edges or links symbolizing a Heisenberg interaction. In the 2D projection (viz., the planar pyrochlore) each tetrahedron is mapped to a square with spins at its vertices, with the sides denoting the NN bonds with Heisenberg exchange bonds of coupling strength J_1 , plus additional exchange bonds of coupling strength J_2 across its diagonals, i.e., now joining next-nearest-neighbour (NNN) bonds in the square-lattice geometry. Each such square is then coupled to others of the same kind by NN J_1 bonds, resulting in the checkerboard pattern shown in figure 1.

The isotropic planar pyrochlore is simply the case $J_2 = J_1$, but it is of considerable interest to study also the anisotropic case when $J_2 \neq J_1$. While the 2D projection of the 3D pyrochlore pattern preserves the vertex-sharing structure, nevertheless one loses the symmetry between the six equivalent bonds on each tetrahedron in the 3D structure when the 2D projection is made. Thus, in the planar pyrochlore the two diagonal bonds of each crossed square are inequivalent to the four bonds on the sides of the square. This subsequent symmetry reduction is thus itself completely consistent with considering the case $J_2 \neq J_1$ of the anisotropic Heisenberg model on the 2D checkerboard lattice or, equivalently, the anisotropic planar pyrochlore. Alternate names are the crossed chain model and the J_1 - J_2 model on the checkerboard lattice.

Most interest to date on the anisotropic planar pyrochlore has focussed on the case when both bonds are AFM in nature (i.e., $J_1 > 0$, $J_2 > 0$). On the other hand, there has also been increasing interest at both the experimental and theoretical levels in quasi-2D magnetic material in which the NN coupling is ferromagnetic ($J_1 < 0$), while NNN coupling is antiferromagnetic ($J_2 > 0$). Examples of such materials include $\text{Pb}_2\text{VO}(\text{PO}_4)_2$ [27–31], $(\text{CuCl})\text{LaNb}_2\text{O}_7$ [32], $\text{SrZnVO}(\text{PO}_4)_2$

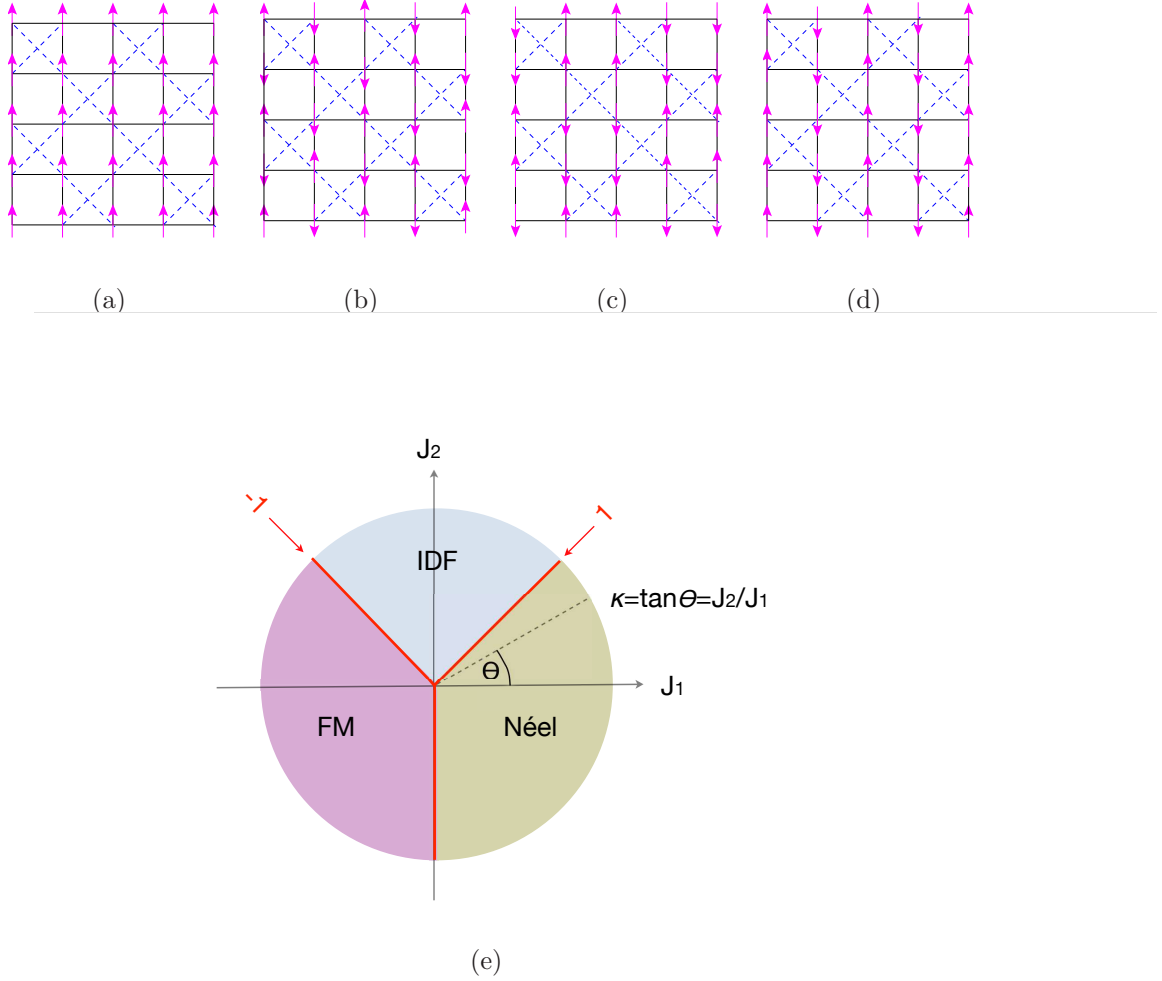


Figure 1. The J_1 - J_2 Heisenberg model on the checkerboard lattice, showing (a) the ferromagnetic (FM) state, (b) the Néel state, (c) one of the two Néel* states, and (d) one (viz., the columnar) of the two striped states. The solid (black) lines are NN J_1 bonds and dashed (green) lines are NNN J_2 bonds. The spins on each lattice site are portrayed by the (brown) arrows. (e) The classical $T = 0$ phase diagram.

[30, 33–35], $\text{BaCdVO}(\text{PO}_4)_2$ [29, 34, 35], $\text{PbZnVO}(\text{PO}_4)_2$ [36] and, $(\text{CuBr})\text{LaNb}_2\text{O}_7$ [37]. Experimental studies of these and other materials have, in turn, stimulated theoretical interest in the GS and thermodynamic properties of the J_1 - J_2 model on the square lattice when the NN exchange bond is FM in nature ($J_1 < 0$) and the NNN exchange bond is AFM, and hence frustrating, in nature ($J_2 > 0$) [38–50]. It is of particular interest to note in this context that there has been a considerable degree of controversy between various theoretical studies on whether or not a magnetically disordered, spin-nematic phase emerges in the spin- $\frac{1}{2}$ model between the phases exhibiting quasiclassical collinear striped AFM order and FM order. In a similar vein we have also recently studied ourselves the spin- $\frac{1}{2}$ J_1 - J_2 - J_3 model on the honeycomb lattice with FM NN

bonds (of strength $J_1 < 0$) and AFM NNN and next-next-nearest-neighbour bonds of equal strength ($J_3 = J_2 > 0$) [51].

Given the high level of interest in the frustrated spin- $\frac{1}{2}$ J_1 - J_2 Heisenberg ferromagnet on the square lattice (i.e., with $J_1 < 0$, $J_2 > 0$) noted above, it seems timely to consider now the analogous model on the checkerboard lattice. In a recent paper [26] we studied the frustrated spin- $\frac{1}{2}$ HAFM on the checkerboard lattice (i.e., with $J_1 > 0$, $J_2 > 0$), using the coupled cluster method (CCM). Our aim now is to extend that analysis to investigate the entire $T = 0$ GS phase diagram, when both exchange couplings J_1 and J_2 can take either sign. After describing and discussing the model itself in section 2, we discuss the CCM methodology in section 3. Our results are then presented in section 4, and we end with a summary and conclusions in section 5.

2. The model

The Hamiltonian for the anisotropic planar pyrochlore is that of a J_1 - J_2 model on a checkerboard lattice. It is written as

$$H = J_1 \sum_{\langle i,j \rangle} \mathbf{s}_i \cdot \mathbf{s}_j + J_2 \sum_{\langle\langle i,k \rangle\rangle} \mathbf{s}_i \cdot \mathbf{s}_k, \quad (1)$$

where the index i runs over all N sites of a square lattice; j runs over all four NN sites to site i that are connected to it by J_1 bonds; and k runs over only two of the NNN sites to site i that are connected to it by J_2 bonds in the checkerboard pattern shown in figure 1. We are interested in the thermodynamic limit ($N \rightarrow \infty$) of an infinite lattice. The sums on $\langle i, j \rangle$ and $\langle\langle i, k \rangle\rangle$ count each pairwise bond once and once only. Thus, the alternate square plaquettes of the checkerboard model have either two NNN (diagonal) bonds (i.e., a cross) or none, as shown in figure 1. Each site i of the lattice carries a particle with a spin quantum number s , defined by a spin operator $\mathbf{s}_i = (s_i^x, s_i^y, s_i^z)$. The checkerboard model is also known as the crossed chain model, which originates from its crossed (in our case, diagonal in figure 1) sets of chains, with J_2 the intrachain exchange coupling constant, and J_1 the (in our case, vertical and horizontal) interchain exchange bonds that connect NN pairs of spins from chains running across one another. We will be interested here in the case $s = 1/2$, but it is worthwhile first to discuss briefly the classical limit ($s \rightarrow \infty$) of the model, in order to compare with the effects caused by quantum fluctuations.

For $J_2 = 0$ the classical GS phase is the FM state shown in figure 1(a) for $J_1 < 0$ and the AFM Néel state shown in figure 1(b) for $J_1 > 0$. Both states are unique for specified values of the ordering vectors. The Néel state has every row and column joined by J_1 bonds with NN spins oriented antiparallel to one another, and hence with each of the diagonal crossed J_2 -chains ordered ferromagnetically with all of the spins on a given diagonal oriented parallel to one another, but with spins on diagonals in a given direction oriented antiparallel to those on the diagonals in the perpendicular direction. Both the Néel and the FM states will clearly remain the stable GS phases in their respective domains for sufficiently small values of $|J_2|$.

The GS energy of the classical Néel state is thus $E_{\text{Néel}}^{\text{cl}}/N = s^2(-2J_1 + J_2)$. Clearly, for sufficiently large values of $J_2 > 0$ the spins on the diagonals (or crossed J_2 -chains) will prefer to align antiferromagnetically. It is trivial to see that there is an infinitely degenerate family (IDF) of collinear AFM phases in which every diagonal J_2 -chain displays Néel AFM ordering, but where every diagonal (each of which is connected by J_1 bonds to two other crossed diagonal J_2 -chains) can be arbitrarily displaced along its own direction or, equivalently, where all of its spins have their directions reversed. All of these states have the same classical energy per spin given by $E_{\text{IDF}}^{\text{cl}}/N = -s^2J_2$, completely independent of the exchange coupling J_1 .

When $J_1 > 0$ there is thus only one classical phase transition in the model, at $\kappa_{\text{cl}}^a = 1$, between the Néel AFM phase and the IDF of AFM phases, where $\kappa \equiv J_2/J_1$ is the frustration (or planar pyrochlore anisotropy) parameter. One particular member of this IDF is the so-called Néel* state [26], (one of which is) shown in figure 1(c). It has doubled AFM order, $\cdots \uparrow\uparrow\downarrow\downarrow\uparrow\uparrow\downarrow\downarrow \cdots$, along each row and column of sites joined by J_1 bonds, such that the single-site \uparrow or \downarrow spin in the Néel state is replaced by the two site $\uparrow\uparrow$ or $\downarrow\downarrow$ unit in the Néel* state. The Néel* state is actually doubly degenerate (for a given direction of the Néel vector), since a translation along a lattice (square-plaquette) diagonal [i.e., a translation of one lattice vector in the horizontal direction plus one lattice vector in the vertical direction of figure 1(c)] transforms one of the pair into the other. Two other simple members of the IDF of classical GS phases for $\kappa > 1$ (and $J_1 > 0$) are the so-called columnar and row striped states [26], the former of which is shown in figure 1(d). These have, respectively, columns or rows of spins joined by J_1 bonds ordered in a FM fashion, with spins on alternating columns or rows oriented antiparallel to one another, and hence with Néel AFM ordering along rows or columns, respectively, for the two cases. Like the Néel* state, the striped states are doubly degenerate (for a given Néel vector), since the row and columnar states transform into one another under interchange of rows and columns.

The GS energy of the classical FM state is $E_{\text{FM}}^{\text{cl}}/N = s^2(2J_1 + J_2)$, and hence there is a second classical phase transition at $\kappa_{\text{cl}}^b = -1$ between the FM state and the IDF of AFM states, when $J_1 < 0$. Finally, there is a third classical phase transition between the Néel AFM state and the FM state at $J_1 = 0$, when $J_2 < 0$ (or, equivalently at $\kappa_{\text{cl}}^c = \pm\infty$, with $J_2 < 0$). In summary we have three classical GS phases, namely (a) the Néel AFM state in the regime $J_1 > 0$ and $-\infty < J_2 < J_1$, (b) the IDF of AFM states for $J_2 > |J_1|$, and (c) the FM state for $J_1 < 0$ and $-\infty < J_2 < -J_1$, all as shown in figure 1(e).

Clearly the model has several interesting special limiting cases. For example, in the case of AFM NN couplings ($J_1 > 0$), the model reduces to the isotropic Heisenberg antiferromagnet (HAFM) on the square lattice as $\kappa \rightarrow 0$, and to decoupled one-dimensional (1D) crossed isotropic HAFM chains as $\kappa \rightarrow \infty$. In between, at $\kappa = 1$, the model is simply the isotropic HAFM on the checkerboard lattice, which is itself a 2D analogue of the 3D isotropic pyrochlore HAFM. Compared to the classical version ($s \rightarrow \infty$) of the model, for which the full GS phase diagram in the J_1 - J_2 plane is known,

the $s = 1/2$ case is basically only well established at precisely the above three points when $J_1 > 0$.

Thus, for the spin- $\frac{1}{2}$ HAFM on the square lattice ($\kappa = 0$) there is a general consensus that the classical Néel AFM LRO is weakened but not destroyed by quantum fluctuations, such that the sublattice magnetization is reduced to about 61.5% of its classical value of 0.5 for the $s = 1/2$ case [52–56]. The excited states are also well established to be gapless integer-spin magnons for the $s = 1/2$ model. One then expects, by continuity, that this (partial) Néel AFM order will persist as the frustrating NNN bonds (with strength $J_2 > 0$) are turned on. As J_2 increases (with $J_1 > 0$ held fixed) we expect that this order will ultimately vanish at some critical value $\kappa = \kappa_{c1}$, where the Néel staggered magnetization becomes zero. In the opposite limit, $\kappa \rightarrow \infty$ (i.e., $J_2 \rightarrow \infty$ with $J_1 > 0$), where we have decoupled 1D isotropic HAFM chains, the model is exactly soluble for the spin- $\frac{1}{2}$ case. The GS phase is a Luttinger spin liquid, in which the quantum fluctuations have completely destroyed the classical Néel LRO, such that the Néel staggered magnetization vanishes. The excited states are gapless, deconfined, spin- $\frac{1}{2}$ spinons.

In between these two limits, at $\kappa = 1$, most studies now concur (and see, e.g., [12, 15, 18, 20, 24–26]) that the GS phase of the $s = 1/2$ isotropic HAFM on the checkerboard lattice is a plaquette valence-bond crystal (PVBC) with quadrumer LRO on isolated spin-singlet square plaquettes, on top of which there is an excitation spectrum of gapped, confined, integer-spin spinons. Again, by continuity, one expects that this PVBC order will persist over a (finite) range of the anisotropy parameter κ on either side of the isotropic value $\kappa = 1$.

On the low- κ side it is still not completely settled whether there is a direct (i.e., first-order in the Landau-Ginzburg scenario) phase transition between the states with Néel AFM order and PVBC order at $\kappa = \kappa_{c1}$, or, if not, there exists an intermediate coexistence phase with both types of ordering and, hence, with two different order parameters. On the high- κ side we expect that PVBC order will persist out to some critical value $\kappa_{c2} > 1$. The situation for $\kappa > \kappa_{c2}$ (with $J_1 > 0$) has been, up till now, the most unsettled part of the phase diagram. Various scenarios have been put forward, as have been summarized in our own earlier paper [26]. In particular, it is an obvious question to ask if any of the IDF of classical ($s \rightarrow \infty$) AFM states that exist for $\kappa > \kappa_{cl}^a = 1$, survives the quantum fluctuations present in the $s = 1/2$ model. Furthermore, if the answer is affirmative, one may then enquire as to whether the classical degeneracy might be lifted by the well-known “order-by-disorder” mechanism [57, 58].

In a recent previous paper [26] we studied the $s = 1/2$ model on the anisotropic checkerboard lattice, using the CCM, in the case when both NN and NNN exchange couplings are AFM in nature (i.e., with $J_1 > 0$, $J_2 > 0$). We used various AFM classical ground states as CCM reference states, including the Néel state of figure 1(b), the Néel* state of figure 1(c), and the (columnar) striped state of figure 1(d). We thereby presented results for the GS energy and average local on-site magnetization (i.e., the

magnetic order parameter) of these states, including their susceptibilities against the formation of both PVBC order and crossed-dimer valence bond crystal (CDVBC) order. The CDVBC state is one with dimer LRO on isolated spin-singlet dimers arranged in a pattern of crossed dimers on alternating square plaquettes (i.e., on every second row and every second column). Our main findings are summarized as follows.

Firstly, we showed that the AFM quasiclassical state with Néel ordering is indeed the GS phase for $\kappa < \kappa_{c_1} \approx 0.80 \pm 0.01$. Secondly, we showed that although quantum fluctuations do indeed lift the classical degeneracy of the IDF of AFM states that form the GS phase for the classical version ($s \rightarrow \infty$) of the model for $\kappa > 1$, with the Néel* states having a lower energy than the striped states, all of these states are actually magnetically unstable in the sense that their magnetic order parameters are zero (or negative) within very small numerical errors. Thirdly, we showed that our calculations preferred instead a PVBC-ordered phase for $\kappa_{c_1} < \kappa < \kappa_{c_2} \approx 1.22 \pm 0.02$, and a CDVBC-ordered phase for *all* values of $\kappa > \kappa_{c_2}$. Lastly, our calculations indicated that both transitions (i.e., from Néel to PVBC, and from PVBC to CDVBC) are probably direct ones. Nevertheless, we could not entirely rule out regions of coexistence in both cases, although we showed that if they do exist they must be very narrow, being confined respectively to $0.79 \lesssim \kappa \lesssim 0.81$ and $1.20 \lesssim \kappa \lesssim 1.22$.

The main purpose of the present paper is now to extend the above analysis to the entire phase space, where both NN and NNN exchange bonds can now be either AFM or FM in nature. A particular aim will be to examine the phase boundary of the CDVBC state when the NN bonds are allowed to become FM (i.e, with $J_1 < 0$).

3. The coupled cluster method

The CCM is a universal method of *ab initio* quantum many-body theory, which is open to systematic step-by-step improvements via various well-defined approximation schemes. It has been applied with considerable success to a wide spectrum of both finite and extended physical systems defined either in a spatial continuum or on a regular discrete lattice [59–65]. These range from atoms and molecules of interest in quantum chemistry to the electron gas; from closed- and open-shell atomic nuclei to infinite nuclear matter; from various strongly interacting quantum field theories to models of interest in quantum optics, quantum electronics and solid-state optoelectronics; as well as to many condensed-matter systems, including highly-frustrated and strongly-correlated spin-lattice systems of the kind considered here.

The CCM is particularly appropriate for such quantum magnets, for which many of the alternative methods have serious drawbacks. For example, quantum Monte Carlo (QMC) techniques are hindered by the well-known minus-sign problem, which is usually unavoidable for frustrated spin-lattice problems. Similarly, the exact diagonalization (ED) method is usually confined to such relatively small finite-lattice clusters that the more subtle orderings present in the GS phase diagram may be difficult to detect and calculate accurately. The CCM suffers from neither of these problems, and has been

applied with great success in recent years to many different spin-lattice models of topical interest in quantum magnetism (and see, e.g., [26, 47, 51, 56, 62, 65–73] and references cited therein).

Since the CCM methodology has been described in detail elsewhere (and see, e.g., [56, 61–65, 67, 70, 72]), we focus only on its key elements here. We note that the method is size-extensive, and can hence provide results in the thermodynamic limit ($N \rightarrow \infty$) from the outset. The first step is always to choose a suitable, normalized N -body model (or reference) state, $|\Phi\rangle$, on top of which the quantum fluctuations present in the exact GS wave function $|\Psi\rangle$ of the phase under study can be incorporated at the next stage, described below. The conditions that $|\Phi\rangle$ must satisfy are also described below. The exact GS ket- and bra-state wave functions, which satisfy the respective Schrödinger equations,

$$H|\Psi\rangle = E|\Psi\rangle; \quad \langle\tilde{\Psi}|H = E\langle\tilde{\Psi}|, \quad (2)$$

are chosen to have normalizations such that $\langle\tilde{\Psi}|\Psi\rangle = \langle\Phi|\Psi\rangle = \langle\Phi|\Phi\rangle = 1$.

A key element of the CCM is then to parametrize these exact states in terms of the chosen model state via the distinctive exponentiated forms,

$$|\Psi\rangle = e^S|\Phi\rangle; \quad \langle\tilde{\Psi}| = \langle\Phi|\tilde{S}e^{-S}. \quad (3)$$

In turn, the two correlation operators, S (\tilde{S}), are themselves formally decomposed in terms of a mutually commuting set of N -body creation operators $\{C_I^+\}$ (annihilation operators $\{C_I^- \equiv (C_I^+)^\dagger\}$), as

$$S = \sum_{I \neq 0} \mathcal{S}_I C_I^+; \quad \tilde{S} = 1 + \sum_{I \neq 0} \tilde{\mathcal{S}}_I C_I^-, \quad (4)$$

where we define $C_0^+ \equiv 1$ to be the identity operator, and where the set index I denotes a complete set of single-particle configurations for all N particles. The model state $|\Phi\rangle$ and the operators $\{C_I^+\}$ must be selected so that $|\Phi\rangle$ is a fiducial (or cyclic) vector with respect to the set of mutually commuting creation operators $\{C_I^+\}$. The model state thus plays the role of a generalized vacuum state, with $\langle\Phi|C_I^+ = 0 = C_I^-|\Phi\rangle, \forall I \neq 0$. Furthermore the set of states $\{C_I^+|\Phi\rangle\}$ spans the entire Hilbert space to which $|\Psi\rangle$ belongs.

For applications to spin-lattice problems it is convenient to consider each lattice site k in the chosen model state $|\Phi\rangle$ to be equivalent to all others. A simple way to do so is to rotate (passively) each spin on each site k separately in such a way that every spin points downward (say along the negative z -direction) in its own local frame of spin axes. Such choices of local spin coordinates leave the basic SU(2) spin commutation relations unchanged. However, all independent-spin product model states thereby take the universal form $|\Phi\rangle = |\downarrow\downarrow\downarrow \cdots \downarrow\rangle$, and the N -body creation operators C_I^+ similarly take a universal product form, $C_I^+ \equiv s_{k_1}^+ s_{k_2}^+ \cdots s_{k_n}^+$, in terms of the single-spin raising operators, $s_k^+ \equiv s_k^x + i s_k^y$. If each site carries a spin with spin quantum number s , no site-index k_j in the product form for C_I^+ may appear more than $2s$ times (i.e., for the present $s = \frac{1}{2}$ case, each index may appear at most once). Clearly the set index I thus

simply becomes $I \equiv \{k_1, k_2, \dots, k_n; n = 1, 2, \dots, 2sN\}$. With the choice of local spin coordinates thus made separately for each model state, the Hamiltonian simply needs to be suitably rewritten in terms of the selected spin-coordinate frames.

The CCM correlation coefficients $\{\mathcal{S}_I, \tilde{\mathcal{S}}_I\}$, which completely determine all GS properties, are now themselves calculated by minimization of the GS energy expectation value functional,

$$\bar{H} = \bar{H}[\mathcal{S}_I, \tilde{\mathcal{S}}_I] \equiv \langle \Phi | \tilde{S} e^{-S} H e^S | \Phi \rangle, \quad (5)$$

with respect to each of the coefficients $\{\mathcal{S}_I, \tilde{\mathcal{S}}_I; \forall I \neq 0\}$. Variation of equation (5) with respect to $\tilde{\mathcal{S}}_I$ from equation (4) yields the coupled set of non-linear equations,

$$\langle \Phi | C_I^- e^{-S} H e^S | \Phi \rangle = 0, \quad \forall I \neq 0, \quad (6)$$

for the set of creation correlation coefficients $\{\mathcal{S}_I\}$. Similarly, variation of equation (5) with respect to \mathcal{S}_I from equation (4) yields the corresponding set of linear equations,

$$\langle \Phi | \tilde{S} e^{-S} [H, C_I^+] e^S | \Phi \rangle, \quad \forall I \neq 0, \quad (7)$$

for the set of annihilation correlation coefficients $\{\tilde{\mathcal{S}}_I\}$, once equation (6) has first been solved for the coefficients $\{\mathcal{S}_I\}$. Since $[S, C_I^+] = 0$ by construction, we note that equation (7) may be re-expressed in the form of a set of generalized linear eigenvalue equations,

$$\langle \Phi | \tilde{S} (e^{-S} H e^S - E) C_I^+ | \Phi \rangle, \quad \forall I \neq 0, \quad (8)$$

for the coefficients $\{\tilde{\mathcal{S}}_I\}$.

The GS energy eigenvalue E , is then just the value of \bar{H} at the minimum determined from solving equations (6) and (7), namely

$$E = \langle \Phi | e^{-S} H e^S | \Phi \rangle = \langle \Phi | H e^S | \Phi \rangle. \quad (9)$$

Similarly, one may find the GS expectation value of any other operator in terms of the coefficients $\{\mathcal{S}_I, \tilde{\mathcal{S}}_I\}$. For example, we may calculate the GS magnetic order parameter M , which is defined to be the average local on-site magnetization,

$$M \equiv -\frac{1}{N} \langle \Phi | \tilde{S} e^{-S} \sum_{l=1}^N s_l^z e^S | \Phi \rangle, \quad (10)$$

where in equation (10) the spins are referred to their local rotated frames.

We note that no approximations have yet been made. However, equations (6) for the coefficients $\{\mathcal{S}_I\}$ are explicitly nonlinear, and one may wonder if truncations of the exponential terms are needed in practice. We note that these appear, in both equations (6) and (8), only in the form of the similarity transformation $e^{-S} H e^S$ of the Hamiltonian. This combination may be expanded in terms of the well-known sum of nested commutators. Another key feature of the CCM is that this otherwise infinite sum will now terminate exactly with the double commutator term. This is due to the basic SU(2) spin commutation relations, together with the fact that all of the terms in equation (4) that comprise the decomposition for the operator S both commute with one another and are simple products of single-spin spin-raising operators. Thus, all

terms in the expansion for $e^{-S}He^S$ are linked, and the Goldstone linked-cluster theorem is exactly preserved even when the expansion of equation (4) for S is truncated in any conceivable way. In turn, this guarantees that the CCM is size-extensive at any such level of truncation, so that we may work in the thermodynamic limit ($N \rightarrow \infty$) from the very beginning. Similar considerations also apply to the evaluation of the GS expectation value of any operator, such as that for the magnetic order parameter M in equation (10).

In practice, therefore, the sole approximation made is to restrict the set of indices $\{I\}$ retained in the expansions of equation (4) for the CCM correlation operators $\{S, \tilde{S}\}$. As in our earlier work [26] on this model, and in many other applications too, we use here the well-tested localized (lattice-animal-based subsystem) LSUB m truncation scheme [26, 47, 56, 62, 67–73], in which at the m th level of approximation we retain only the multispin-flip configurations $\{I\}$ in equation (4) that are defined by at most m contiguous lattice sites. A cluster configuration is defined to be contiguous in this sense if every site in the cluster is adjacent (or connected) in the NN sense (in the selected geometry) to at least one other site in the cluster.

The number of such fundamental LSUB m configurations, $N_f = N_f(m)$, may be reduced by incorporating the space- and point-group symmetries of the Hamiltonian and model state being used, as well as any conservation laws that similarly pertain to both. Nevertheless, the number $N_f(m)$ is a rapidly increasing function of the truncation index m , and hence the need soon arises to utilize massive parallelization plus supercomputing resources for the highest-order calculations we undertake [67, 74]. For the present checkerboard model we employ both the Néel and Néel* states shown in figures 1(b) and 1(c), respectively, as our CCM model states. We also use the basic checkerboard geometry to define the LSUB m configurations, in the sense that we treat both the pairs of sites connected by J_1 bonds as well as those connected by J_2 bonds as being contiguous sites. For both model states we are able to perform LSUB m calculations with values of the truncation index $m \leq 10$.

It is worth noting that if we were to use the basic square-lattice geometry (i.e., with LSUB m contiguous sites defined only by those joined by J_1 bonds), the number $N_f(m)$ of fundamental configurations would be considerably smaller than in the checkerboard geometry, at the same LSUB m level. In turn, this could possibly permit us to perform higher-order LSUB m calculations with the same level of computational resource. However, this possible advantage is accompanied by the severe drawback that the LSUB m sequences of approximations for both E/N and M now display a marked staggering effect in $m \equiv 2k$, depending on whether the index k is now odd or even. The reason for such a staggering behaviour is clearly due to the fact that the full LSUB m sequence using the square-lattice geometry does not properly reflect the checkerboard-lattice symmetries. Such odd-even staggering effects in index m have been observed previously in CCM LSUB m approximations for simple (dynamically unfrustrated) models [75]. It always has the undesirable consequence of making extrapolations (for the full sequence) to the exact $m \rightarrow \infty$ limit much more difficult and much less robust.

Thus, finally, the only remaining step (and the only approximation made in the whole CCM procedure) is to extrapolate our LSUB m sequences of approximants for a given GS parameter to the limit $m \rightarrow \infty$ where the method is exact. For the GS energy we use the usual, well-tested extrapolation scheme [26, 47, 56, 65, 69–73, 75],

$$E(m)/N = a_0 + a_1 m^{-2} + a_2 m^{-4}. \quad (11)$$

For highly frustrated magnetic systems, particularly ones which are close to a quantum critical point (QCP) or for which the magnetic order parameter M is close to zero, the extrapolation scheme which has been found to be appropriate in many earlier studies (see, e.g., [26, 47, 56, 69, 71–73]) is one with a leading exponent $1/m^{1/2}$,

$$M(m) = c_0 + c_1 m^{-1/2} + c_2 m^{-3/2}. \quad (12)$$

We note finally that, without making any truncation (e.g., by using the LSUB m scheme utilized here), the solutions to equations (6) and (8) are formally exact, and hence independent, in principle, of the reference state $|\Phi\rangle$ used (at least as long, for example, as $|\Phi\rangle$ shares the same quantum numbers as the exact state $|\Psi\rangle$). The only caveat is that this assumes intrinsically that a solution (to the full, untruncated CCM equations) exists for a given choice of model state $|\Phi\rangle$. In practice, of course, approximations must be made, e.g., by using the LSUB m scheme advocated above. Then, of course, the solutions at a given LSUB m level of truncation for $|\Psi\rangle$ may well, in principle, depend on the reference state $|\Phi\rangle$. As discussed more fully below in section 4, the range of values of the Hamiltonian parameters for which the truncated equations have a solution usually does, in practice, depend both on the choice of $|\Phi\rangle$ and the order m of the truncation. So long as the scaling procedure to the $m \rightarrow \infty$ limit would be exact, the dependence on $|\Phi\rangle$ would then be removed. In practice, since the scaling laws are empirical, the best we can expect is that any remaining dependence on any states $|\Phi\rangle$ for which solutions to the CCM equations exist in the same parameter range will be only very weak.

4. Results

We now present our CCM results separately for the two cases when the model state is chosen to be the Néel state or the Néel* state.

4.1. Néel model state; Néel phase boundaries

In our previous paper on the spin- $\frac{1}{2}$ anisotropic planar pyrochlore [26] we set $J_1 = +1$ to set the energy scale for the case of AFM NN bonds, and employed the Néel state as our CCM model state in order to investigate the QCP at which Néel order vanishes as we turn on and strengthen NNN bonds with a frustrating exchange coupling of strength $J_2 \equiv \kappa J_1 > 0$. In particular, we calculated the magnetic order parameter M at various LSUB m levels of approximation for $m \leq 10$, for values of the frustration parameter κ in the range $0 \leq \kappa < \kappa^t(m)$. Here, $\kappa^t(m)$ is the highest value for κ for which, at a given LSUB m level of approximation, a real solution to the CCM equations (6)

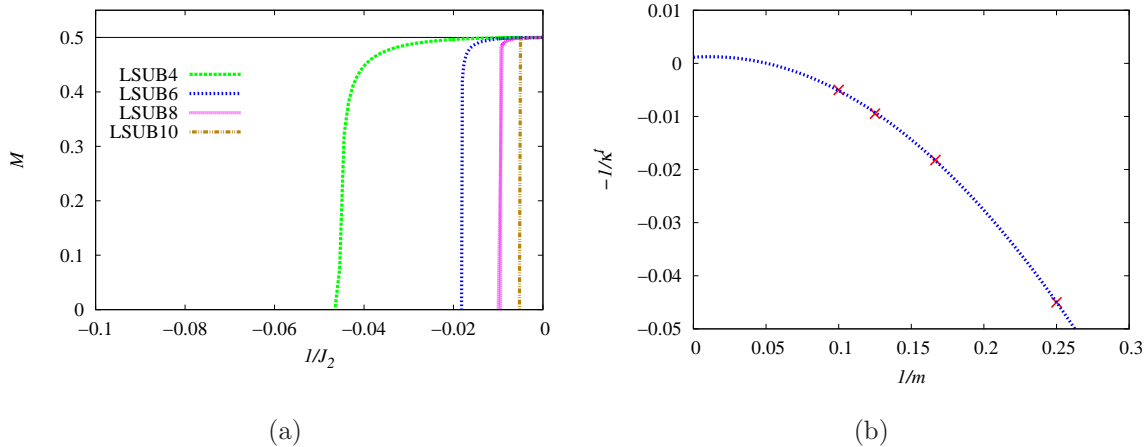


Figure 2. (a) Ground-state magnetic order parameter, M , for the Néel state of the spin- $\frac{1}{2}$ J_1 - J_2 checkerboard model (with $J_1 = -1$, $J_2 < 0$) as a function of $1/J_2 \equiv -1/\kappa$. The CCM results for various LSUB m approximations with $m = 4, 6, 8, 10$ are shown. (b) The scaling of the LSUB m termination points $\kappa^t(m)$ in figure 2(a) as a function of $1/m$, is shown according to equation (13).

could be found. Such termination points are by now well understood. They have been shown [47, 65, 70] to be direct manifestations of the associated QCP at which the order of the model state melts in the physical system under study. As is typically the case, we found that the corresponding values of $\kappa^t(m)$ are greater than the associated critical value κ_{c_1} ($\approx 0.80 \pm 0.01$), and that they approach κ_{c_1} monotonically (as a function of m) from above.

We now turn our attention first to the case when the NNN bonds become FM in nature (i.e., $J_2 < 0$), still keeping $J_1 = +1$. Clearly, the two bonds no longer frustrate one another and we fully expect the Néel order to be preserved in such a way that the order parameter M monotonically increases as $|J_2|$ increases, with $M \rightarrow \frac{1}{2}$ as $J_2 \rightarrow -\infty$. Then, as the strength J_1 of the NN bonds changes sign in the same limit $J_2 \rightarrow -\infty$, the stable GS phase will clearly become the FM phase via a first-order transition. Since the FM states (of both the entire lattice and the decoupled crossed 1D chains in this limit) are exact eigenstates of the Hamiltonian of equation (1) for all values of the spin quantum number s , the phase boundary between the Néel and FM phases is expected to be the same for the quantum case as in figure 1(e) for the classical ($s \rightarrow \infty$) case.

Nevertheless, it is of interest to see how our CCM LSUB m solutions based on the Néel state as model state actually conform to the above expectation. Accordingly, we show in figure 2(a) the LSUB m results for the magnetic order parameter M , for the cases $m = \{4, 6, 8, 10\}$, with $J_1 = -1$, $J_2 < 0$. We see once again very clearly that the LSUB m results based on the Néel state terminate slightly into the FM regime, with the corresponding lower termination points monotonically approaching the Néel-FM boundary at $\kappa_{c_4} = \infty$ as $m \rightarrow \infty$. The actual values of the inverse of the lower LSUB m termination points, $1/\kappa^t(m)$, are +0.045, +0.0182, +0.00948 and +0.00500

for $m = 4, 6, 8$, and 10 , respectively. Clearly, any reasonable extrapolation scheme is compatible with $1/\kappa^t(\infty) = 0$. For example, the scheme

$$1/\kappa^t(m) = \alpha_0 + \alpha_1 m^{-1} + \alpha_2 m^{-2}, \quad (13)$$

shown in figure 2(b), yields the value $\alpha_0 = -0.0011 \pm 0.0019$, where the error is simply that associated with the fit to the four values $m = \{4, 6, 8, 10\}$.

The fact that we find solutions of the CCM LSUB m equations based on the Néel state as reference state (with a non-vanishing value of the Néel order parameter) for small negative values of J_2 (i.e., intruding slightly into the FM regime), is related to the fact that our solutions are thus intrinsically biased towards the stability of the Néel phase. As one proceeds to higher LSUB m orders (i.e., as the index m is increased) the region of unphysical intrusion decreases, and vanishes in the $m \rightarrow \infty$ limit, as may clearly be observed in figure 2(a). This is a completely general feature of CCM LSUB m solutions, which has been observed in many previous CCM studies of quantum magnets. In general, if the stable GS phase (say, B) in the physical intrusion region based on a given CCM reference state (say, A) is itself amenable to a CCM solution based on another (typically classical) reference state B , then we would also typically find a similar region of unphysical intrusion of the latter B -phase solution into the physical A -phase region. However, in the present case, since the FM wave function illustrated in figure 1(a) is itself an exact eigenstate of our Hamiltonian of equation (1), it cannot be used as a CCM reference state, except in the trivial sense that all (exact or approximate) solutions based on it simply yield vanishing values of all of the correlation coefficients $\{\mathcal{S}_I, \tilde{\mathcal{S}}_I\}$ retained in equation (4).

4.2. Néel* model state; CDVBC phase boundaries

We now turn to our corresponding LSUB m results based on the Néel* state of figure 1(c) as the CCM model state. In our previous paper [26] we investigated the case of AFM NN bonds ($J_1 = +1$), and we now similarly consider the case of FM NN bonds ($J_1 = -1$). In both cases we investigate the effect of frustrating AFM NNN bonds ($J_2 > 0$).

Results for the ground-state energy per spin, E/N , for both cases ($J_1 = -1$ and $J_1 = +1$), are shown in figure 3. Figure 3(a) shows the “raw” LSUB m results for values of the truncation index $m = 4, 6, 8, 10$, while figure 3(b) shows extrapolated LSUB ∞ results using equation (11). We also show the exact result for the FM phase for the present $s = \frac{1}{2}$ model, $E_{\text{FM}}/N = \frac{1}{4}(2J_1 + J_2)$, with $J_1 = -1$. In figure 3 the curves without symbols attached refer to our present case ($J_1 = -1$), while the corresponding curves with symbols attached refer to the case $J_1 = +1$. They are taken from our earlier work [26], and are shown for the sake of comparison.

Figure 3(a) clearly shows that the LSUB m results for the GS energy converge extremely rapidly in both cases as m is increased. Furthermore, we see that for all values $J_2 \gtrsim 1.5$ the results for both cases are remarkably similar. Nevertheless, important qualitative differences emerge for small values of J_2 , in the vicinity of the corresponding

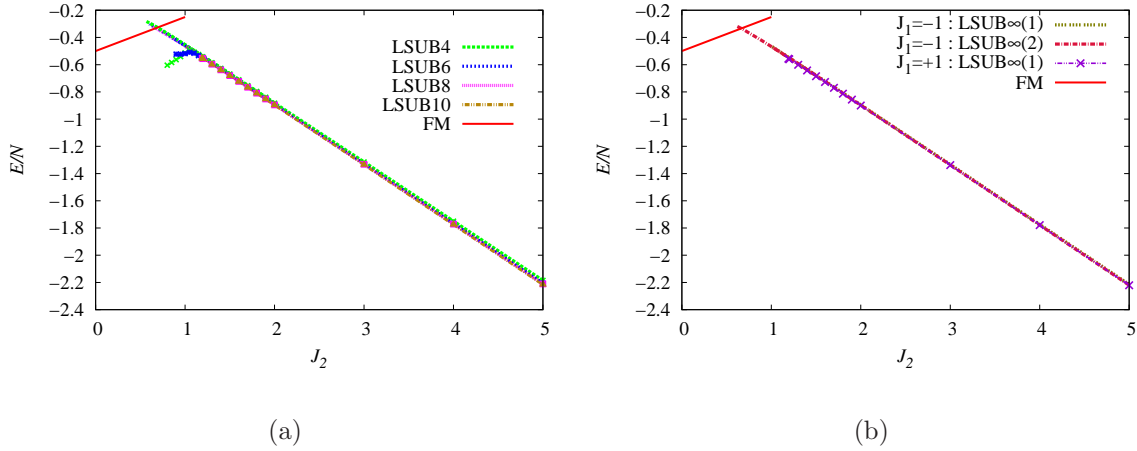


Figure 3. CCM results for the GS energy per spin, E/N , for the spin- $\frac{1}{2}$ J_1 - J_2 Heisenberg model on the checkerboard lattice. (a) LSUB m results with $m = 4, 6, 8, 10$ based on the Néel* state. Results without symbols attached refer to the case $J_1 = -1$, and are compared to the corresponding results for the case $J_1 = +1$, shown with symbols attached. The GS energy per spin, $E/N = (J_2 - 2)/4$, for the FM phase is also shown. (b) The extrapolated results using equation (11): LSUB ∞ (1) uses the data sets $m = \{4, 6, 8, 10\}$ and LSUB ∞ (2) uses the data sets $m = \{2, 4, 6, 8\}$.

classical phase transitions at $J_2 = 1$ in both cases, as shown in figure 1(e). In figure 3(a) both sets of results are shown out to their respective (approximately determined) termination points, $|\kappa^t(m)|$. It is evident that the value of $|\kappa^t(m)|$ for a given value of m is always less in the case $J_1 = -1$ than in the case $J_1 = +1$. As we showed previously [26], in the case $J_1 = +1$, the values $\kappa^t(m) \rightarrow \kappa_{c_2} \approx 1.22 \pm 0.02$ as $m \rightarrow \infty$.

By contrast, the respective LSUB m values of $\kappa^t(m)$ based on the Néel* state in the case $J_1 = -1$ are $\kappa^t(4) \approx -0.56$, $\kappa^t(6) \approx -0.60$, and $\kappa^t(8) \approx -0.63$. These termination points are themselves very close to the corresponding values where the GS energy curves cross that of the FM state, $\kappa^e(4) \approx -0.692$, $\kappa^e(6) \approx -0.677$, and $\kappa^e(8) \approx -0.671$. Once again, as the LSUB m truncation index m is increased to infinity, the size of the region in which our solutions extend into the FM regime diminishes to zero, and we expect that $\kappa^t(\infty) = \kappa^e(\infty) = \kappa_{c_3}$.

We note, however, that it is computationally very costly to determine the values $\kappa^t(m)$ with high accuracy, since the CCM LSUB m solutions require increasingly greater amounts of computational resource, for a specified level of accuracy, the closer a termination point is approached. For this reason the values $\kappa^e(m)$ are appreciably more accurate than the corresponding values $\kappa^t(m)$. We also note that, for the same reason, we have been unable to track the LSUB10 solution based on the Néel* state, in the case $J_1 = -1$, down to values sufficiently close to $\kappa^t(10)$ for the respective energy curve to have crossed the FM energy curve. A simple extrapolation of the energy crossing points $\kappa^e(m)$, using a scheme of the form of equation (11) and the LSUB m values with $m = \{4, 6, 8\}$ yields a value $\kappa_{c_3} \approx -0.661$ for the QCP. A similar extrapolation using

the data set $m = \{3, 5, 7\}$ gives the value $\kappa_{c_3} \approx -0.662$.

While it is certainly true that three-parameter fits to only three m -value points, as quoted above, are intrinsically dangerous, the energy curves themselves are very smooth, even near the critical point κ_{c_3} , as one can see clearly from figure 3. Hence, we may have considerable confidence in the quoted values. However, to verify this point we may also use the extrapolated curve based on the Néel* state with the four-point data set $m = \{4, 6, 8, 10\}$. Since the calculated LSUB10 curve now terminates before the crossing point with the FM energy curve, the resulting extrapolated Néel* energy curve must itself be extrapolated the short distance to the crossing point, which introduces an additional error. Nevertheless, since the curve itself is again very smooth, and indeed almost linear over the entire range of J_2 values shown in figure 3(b), such an extrapolation (e.g., using simple polynomial fits) is, in fact, rather robust (e.g., with respect to the order of the fitting polynomial used). The resulting values of κ_{c_3} for fits using polynomials between third and sixth orders, for example, all lie in the range -0.67 to -0.68. They are thus compatible with the (more accurate) values obtained above from the two fits using three m -values, which require no such extrapolation to the crossing point. Such considerations, together with a more detailed error analysis, leads us to our CCM estimate $\kappa_{c_3} = -0.66(1)$.

We observe from figure 3(b) that the energy curves rapidly approach the $J_2 \rightarrow \infty$ limit of uncoupled spin- $\frac{1}{2}$ 1D HAFM crossed chains, even for values of $J_2 \gtrsim 2$. For example, the extrapolated value of the energy per spin in the regime $4 \leq J_2 \leq 5$ is $E/N \approx -0.4420J_2$, which already is in excellent agreement with the exact asymptotic result, $E/N = (\frac{1}{4} - \ln 2)J_2 \approx -0.4431J_2$ from the Bethe ansatz solution [76,77]. Indeed, if we were to include this curve in figure 3(b) it would lie virtually on top of the extrapolated LSUB ∞ curves, over the whole of the range $1 < J_2 < 5$, and deviating only very slightly from them for values $J_2 \lesssim 1$.

Although we have been able to use the Néel* state completely successfully as a CCM model state, we now need to investigate the stability of the quasiclassical magnetic LRO in the regimes in which we have used it. To that end we now show in figure 4(a) the corresponding results for the GS magnetic order parameter, M , to those shown in figure 3(a) for the GS energy per spin, E/N . It is clear that the CCM LSUB m results for M converge considerably more slowly as a function of the truncation parameter m than do those for E/N , as is to be expected by a comparison of the respective extrapolation schemes of equations (12) and (11). Once again, just like the previous results for E/N in figure 3(a), the corresponding results for M in figure 4(a) are seen to be remarkably similar for the two cases $J_1 = -1$ and $J_1 = +1$ in the region $J_2 \gtrsim 2$. The divergence between the two cases for values $J_2 \lesssim 2$ is completely consistent with our previous discussion for the GS energy results.

In our earlier work [26] for the case $J_1 = +1$ we showed that the rapid rise and then precipitous fall in each of the LSUB m results for M , as J_2 approaches the corresponding termination point for that solution, is a clear marker of the associated QCP at $\kappa_{c_2} \approx 1.22$. Similarly, the analogous behaviour seen in figure 4(a) for the LSUB m results for M for

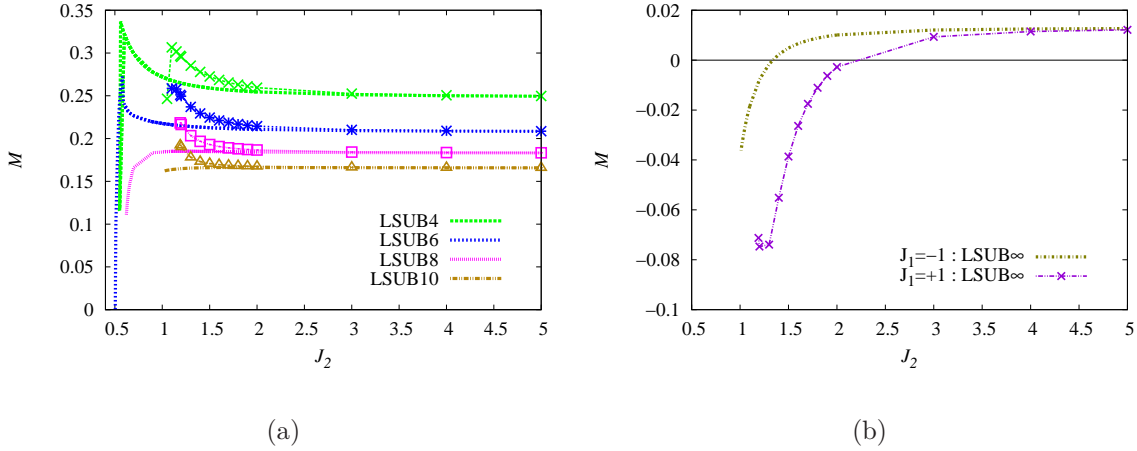


Figure 4. CCM results for the GS magnetic order parameter, M , for the spin- $\frac{1}{2}$ J_1 - J_2 Heisenberg model on the checkerboard lattice. (a) LSUB m results with $m = 4, 6, 8, 10$ based on the Néel* state. Results without symbols attached refer to the case $J_1 = -1$, and are compared to the corresponding results for the case $J_1 = +1$, shown with symbols attached. (b) The corresponding extrapolated results using equation (12) and the data sets $m = \{4, 6, 8, 10\}$.

the present case $J_1 = -1$ is evidently associated with the QCP at $\kappa_{c3} \approx -0.66$ that we have found above in the corresponding results for the GS energy.

In figure 4(b) we show the respective extrapolated LSUB ∞ results for M for the two cases, as obtained from the scheme of equation (12), used with the respective LSUB m data sets with $m = \{4, 6, 8, 10\}$. We see that M is either zero (or very close to zero) or negative over the entire range shown in figure 4, in both cases $J_1 = -1$ and $J_1 = +1$. Our results are, in particular, completely compatible with M being zero in both cases in the asymptotic limit $J_2 \rightarrow \infty$. This is precisely the exact result for this asymptotic (Luttinger spin-liquid) limit of decoupled 1D HAFM chains. We thus conclude that the Néel* state is unlikely to be the stable GS phase for any values of the parameters J_1 and J_2 for which we have, nevertheless, successfully been able to use it as a CCM model state.

Using techniques that combine renormalization group ideas, plus 1D bosonization and current algebra methods, together with a careful analysis of the relevant terms near the delicate Luttinger liquid fixed point of the 1D HAFM spin chain, Starykh *et al.* [20] showed that in the large- κ limit the stable GS phase exhibits spontaneous dimerization. The GS phase in this limit has CDVBC order with twofold spontaneous symmetry breaking, which comprises a staggered ordering of dimers along the crossed J_2 chains (i.e., along the diagonals in figure 1). This finding of a CDVBC state with no magnetic order was then independently confirmed [22, 23] in an analysis using a SE technique based on the flow equation method.

It is thus of interest to investigate within our present CCM analysis whether the

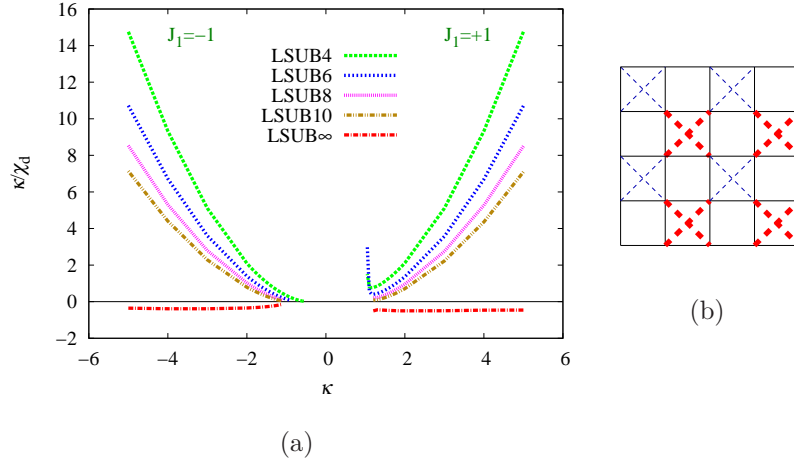


Figure 5. (a) CCM results for the scaled inverse crossed-dimer susceptibility, κ/χ_d , as a function of the frustration parameter, $\kappa \equiv J_2/J_1$, using the Néel* state as the CCM model state, for the spin- $\frac{1}{2}$ J_1 - J_2 Heisenberg model on the checkerboard lattice with $J_1 = -1$ (left curves), comparing with those for $J_1 = +1$ (right curves) (with $J_2 > 0$ for both cases). We also show the extrapolated LSUB ∞ results based on equation (16) with the data sets $m = \{4, 6, 8, 10\}$ as input. (b) The perturbations (fields) $F = \delta \hat{O}_d$ for the dimer susceptibility χ_d . Thick (red) dashed and thin (blue) dashed lines correspond respectively to strengthened and weakened NNN exchange couplings, where $\hat{O}_d = \sum_{\langle\langle i,k \rangle\rangle} a_{ik} \mathbf{s}_i \cdot \mathbf{s}_k$, and the sum runs over the NNN diagonal bonds of the checkerboard lattice, with $a_{ik} = +1$ and -1 for thick (red) dashed and thin (blue) dashed lines respectively. The original solid (black) J_1 bonds are unaltered in strength.

whole (or part) of the regime that has been accessible to us using the Néel* state as model state, but for which we have shown has no Néel* magnetic LRO, might in fact have CDVBC order instead. To that end we consider the response of the system when a field operator, $F = \delta \hat{O}_d$, is added as a small perturbation to the original Hamiltonian of equation (1), with δ an infinitesimally small c -number, and the operator \hat{O}_d , illustrated in figure 5(b), promotes the formation of CDVBC order.

Thus, we now calculate the perturbed GS energy per spin, $e(\delta) \equiv E(\delta)/N$, for the perturbed Hamiltonian, $H(\delta) \equiv H + F$, at various LSUB m levels of approximation, using the Néel* state as our model state. We then calculate the corresponding susceptibility coefficient,

$$\chi_d \equiv - \left. \frac{\partial^2 e(\delta)}{\partial \delta^2} \right|_{\delta=0}, \quad (14)$$

which is a measure of the susceptibility of the system against the formation of CDVBC order. Clearly, χ_d can be used to find points or regions in phase space where the phase corresponding to the particular CCM model state used (viz., here the Néel* state) becomes unstable with respect to a CDVBC-ordered state, namely when the extrapolated inverse susceptibility, $1/\chi_d$, goes to zero.

In order to extrapolate our LSUB m results to the LSUB ∞ limit, it has been found [78, 79] that the simple scheme,

$$\chi_d^{-1}(m) = x_0 + x_1 m^{-2} + x_2 m^{-4}, \quad (15)$$

gives excellent fits, except in regions where χ_d^{-1} becomes very small or zero. In the present case we are, of course, interested in precisely such regimes, and it is then preferable [72, 78, 79] to use an unbiased extrapolation scheme of the form,

$$\chi_d^{-1}(m) = y_0 + y_1 m^{-\nu}, \quad (16)$$

where the leading exponent ν is itself a fitting parameter, together with the coefficients y_0 and y_1 .

We show our results for χ_d^{-1} in figure 5(a). Since the GS energy scales linearly with J_2 in the large J_2 limit, as seen from figure 3, it is more appropriate to show our CCM results in figure 5(a) for the scaled inverse dimer susceptibility, κ/χ_d , as a function of κ . Figure 5(a) shows results for both the cases $J_1 = -1$ and $J_1 = +1$. It is evident from LSUB ∞ extrapolations using equation (16) that our results in both cases are completely consistent with $1/\chi_d$ being zero for all values of κ shown. In other words, our results strongly indicate that everywhere we have been able to use the Néel* state as a CCM model state it is actually unstable against the formation of CDVBC order, which forms the ordering of the true stable GS phase in these regimes. Hence, we conclude that at $\kappa_{c_2} = 1.22 \pm 0.02$ there is a QCP between states with PVBC and CDVBC forms of order, and at $\kappa_{c_3} = -0.66 \pm 0.01$ there is a QCP between states with CDVBC and FM forms of order.

5. Summary and conclusions

In this and our previous paper [26] we have used the CCM, implemented to high orders, to study the spin- $\frac{1}{2}$ J_1 - J_2 Heisenberg model on the checkerboard lattice. Whereas in our earlier work, we studied the model only in the case where both NN and NNN bonds were AFM in nature ($J_1 > 0, J_2 > 0$), we have now investigated the model over the entire J_1 - J_2 phase space. Previously we showed that the classical phase transition at $\kappa_{cl}^a = 1$ ($J_1 > 0$) between the Néel AFM phase and the IDF of AFM phases, is split in the $s = \frac{1}{2}$ model into two transitions at $\kappa_{c_1} = 0.80 \pm 0.01$ and $\kappa_{c_2} = 1.22 \pm 0.02$. For $\kappa < \kappa_{c_1}$ the Néel order persists, while for $\kappa_{c_1} < \kappa < \kappa_{c_2}$ the GS phase has PVBC order. Finally, we showed that for $\kappa > \kappa_{c_2}$ (with $J_1 > 0$) the stable GS phase has CDVBC order. The transitions at both QCPs κ_{c_1} and κ_{c_2} are likely to be direct ones, although we cannot exclude very narrow coexistence regions confined to $0.79 \lesssim \kappa \lesssim 0.81$ and $1.20 \lesssim \kappa \lesssim 1.22$, respectively.

We have now confirmed that the CDVBC phase persists when the J_1 bonds become FM in nature ($J_1 = -1$) to a QCP at $\kappa_{c_3} = -0.66 \pm 0.01$, at which point the CDVBC phase gives way to the FM phase. This QCP may be compared with the corresponding transition in the classical ($s \rightarrow \infty$) model at $\kappa_{cl}^b = -1$ between the IDF of AFM states and the FM state. It is interesting to note that quantum fluctuations act to destabilize

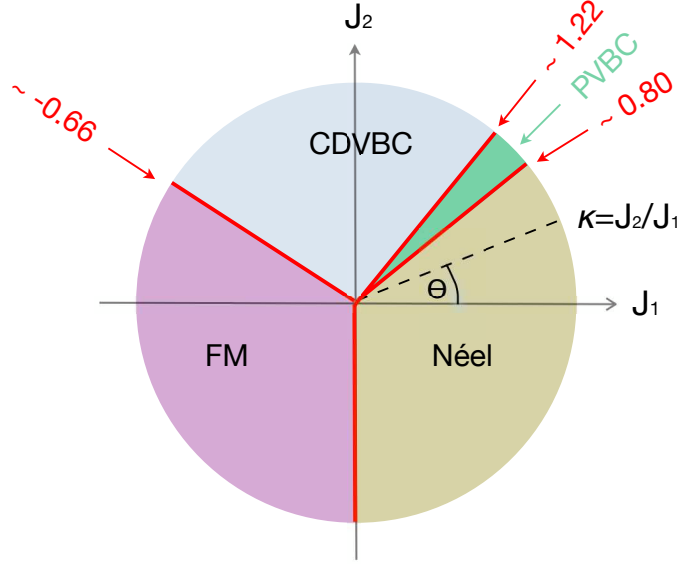


Figure 6. The ground-state ($T = 0$) phase diagram of the spin- $\frac{1}{2}$ J_1 - J_2 Heisenberg model on a checkerboard lattice (with $\kappa \equiv J_2/J_1 \equiv \tan\theta$), showing the Néel antiferromagnetic phase, the plaquette valence-bond crystalline (PVBC) phase, the crossed-dimer valence-bond crystalline (CDVBC) phase, and the ferromagnetic (FM) phase. All of the transitions at $\kappa_{c_1} \approx 0.80(2)$, $\kappa_{c_2} \approx 1.22(2)$, and $\kappa_{c_3} \approx -0.66(1)$, each with $J_2 > 0$, appear to be direct ones. The direct first-order transition between the FM and Néel phases is exactly at $\theta_{c_4} = \frac{3}{2}\pi$.

the FM ordering at a weaker level of frustration than for the classical version of the model. Precisely the same effect has now also been seen in a variety of other comparable models, such as the spin- $\frac{1}{2}$ J_1 - J_2 model on the square lattice [47], the spin- $\frac{1}{2}$ J_1 - J_2 - J_3 model (with $J_3 = J_2$) on the honeycomb lattice [80], and the spin- $\frac{1}{2}$ J_1 - J_2 model on a cross-stripped square lattice [72]. Finally, in the unfrustrated region where $J_2 < 0$, the QCP between the FM and Néel phases has been shown to occur at $\kappa_{c_4} = \infty$, at exactly the same place as in the classical model ($\kappa_{c_4}^c$), fully as expected. Our results are summarized in the complete GS ($T = 0$) phase diagram shown in figure 6.

We note that there have been suggestions in the literature [39, 40, 44, 45, 49] that the competition between FM interactions between NN pairs of spins ($J_1 > 0$) and AFM interactions between other pairs of spins in frustrated spin- $\frac{1}{2}$ systems on the square lattice might result in gapless spin-liquid states with multipolar order (e.g., spin-nematic states) near to the FM boundary. Similar states have also been hypothesised in frustrated multiple cyclic spin-exchange models on the triangular lattice with FM NN pairwise interactions [49], either in a nonzero external magnetic field (with octupolar

ordering occurring) or in zero field (with quadratic or nematic ordering occurring in a state bordering the FM phase). Nevertheless, such states with multipolar-ordering in the zero-field case are deemed to be quite fragile. Indeed, a recent careful and accurate analysis of the spin- $\frac{1}{2}$ FM version of the J_1 - J_2 Heisenberg model (i.e., with $J_1 < 0$) on the square lattice [47], which used both high-order CCM and ED techniques, found that if such states did exist (and no evidence at all was found for them in this study), they could exist only over a very small range below $J_2 \approx 0.4|J_1|$, where the transition at which FM ordering disappears was accurately determined to be $J_2^c = 0.394(1)|J_1|$. A recent Schwinger boson study of the same model [81] also found no evidence for any such states.

Similarly, in our present study of the checkerboard model we have found no evidence at all to suggest that the CDVBC phase does not extend all the way down to the FM phase. Again, if any such intermediate phase exists at all, it would need to be confined to a very small range below $J_2 \approx 0.7|J_1|$, on all the evidence presented here, where the transition at which FM ordering disappears is $J_2^{c3} = 0.66(1)|J_1|$. On the other hand, the detection of phases with novel quantum ordering, such as spin-nematic states, is subtle, and the present checkerboard model may merit further investigation in this respect in the very narrow region just above the border of the FM phase.

Finally, we note that there has been interest shown in frustrated ferromagnets with respect to the formation of multimagnon bound states under the influence of high magnetic fields (and see, e.g., [39, 82–84]). It might, therefore, be of interest to investigate the present checkerboard model further, by coupling it to an external magnetic field.

Acknowledgment

We thank the University of Minnesota Supercomputing Institute for the grant of supercomputing facilities.

References

- [1] Sachdev S 1995 *Low Dimensional Quantum Field Theories for Condensed Matter Physicists* ed Lu Y, Lundqvist S and Morandi G (Singapore: World Scientific)
- [2] Schollwöck U, Richter J, Farnell D J J and Bishop R F (eds) 2004 *Quantum Magnetism (Lecture Notes in Physics vol 645)* (Berlin: Springer-Verlag)
- [3] Misguich G and Lhuillier C 2005 *Frustrated Spin Systems* ed Diep H T (Singapore: World Scientific) p 229
- [4] Anderson P W 1973 *Mater. Res. Bull.* **8** 153
- [5] Singh R R P, Starykh O A and Freitas P J 1998 *J. Appl. Phys.* **83** 7387
- [6] Canals B and Lacroix C 1998 *Phys. Rev. Lett.* **80** 2933–2936
- [7] Palmer S E and Chalker J T 2001 *Phys. Rev. B* **64** 094412
- [8] Brenig W and Honecker A 2002 *Phys. Rev. B* **65** 140407(R)
- [9] Canals B 2002 *Phys. Rev. B* **65** 184408
- [10] Starykh O A, Singh R R P and Levine G C 2002 *Phys. Rev. Lett.* **88** 167203
- [11] Sindzingre P, Fouet J B and Lhuillier C 2002 *Phys. Rev. B* **66** 174424

- [12] Fouet J B, Mambrini M, Sindzingre P and Lhuillier C 2003 *Phys. Rev. B* **67** 054411
- [13] Fukazawa H, Yanagishima D, Higashinaka R and Maeno Y 2003 *Acta Phys. Pol. B* **34** 1501
- [14] Berg E, Altman E and Auerbach A 2003 *Phys. Rev. Lett.* **90** 147204
- [15] Tchernyshyov O, Starykh O A, Moessner R and Abanov A G 2003 *Phys. Rev. B* **68** 144422
- [16] Moessner R, Tchernyshyov O and Sondhi S L 2004 *J. Stat. Phys.* **116** 755
- [17] Hermele M, Fisher M P A and Balents L 2004 *Phys. Rev. B* **69** 064404
- [18] Brenig W and Grzeschik M 2004 *Phys. Rev. B* **69** 064420
- [19] Bernier J S, Chung C H, Kim Y B and Sachdev S 2004 *Phys. Rev. B* **69** 214427
- [20] Starykh O A, Furusaki A and Balents L 2005 *Phys. Rev. B* **72** 094416
- [21] Schmidt H J, Richter J and Moessner R 2006 *J. Phys. A: Math. Gen.* **39** 10673
- [22] Arlego M and Brenig W 2007 *Phys. Rev. B* **75** 024409
- [23] Arlego M and Brenig W 2009 *Phys. Rev. B* **80** 099902(E)
- [24] Moukouri S 2008 *Phys. Rev. B* **77** 052408
- [25] Chan Y H, Han Y J and Duan L M 2011 *Phys. Rev. B* **84** 224407
- [26] Bishop R F, Li P H Y, Farnell D J J, Richter J and Campbell C E 2012 *Phys. Rev. B* **85** 205122
- [27] Kaul E E, Rosner H, Shannon N, Shpanchenko R V and Geibel C 2004 *J. Magn. Magn. Mater.* **272-276** 922
- [28] Skoulatos M, Goff J P, Shannon N, Kaul E E, Geibel C, Murani A P, Enderle M and Wildes A R 2007 *J. Magn. Magn. Mater.* **310** 1257
- [29] Carretta P, Filibian M, Nath R, Geibel C and King P J C 2009 *Phys. Rev. B* **79** 224432
- [30] Skoulatos M, Goff J P, Geibel C, Kaul E E, Nath R, Shannon N, Schmidt B, Murani A P, Deen P P, Enderle M and Wildes A R 2009 *Europhys. Lett.* **88** 57005
- [31] Nath R, Furukawa Y, Borsa F, Kaul E E, Baenitz M, Geibel C and Johnston D C 2009 *Phys. Rev. B* **80** 214430
- [32] Kageyama H, Kitano T, Oba N, Nishi M, Nagai S, Hirota K, Viciu L, Wiley J B, Yasuda J, Baba Y, Ajiro Y and Yoshimura K 2005 *J. Phys. Soc. Jpn.* **74** 1702
- [33] Tsirlin A A and Rosner H 2009 *Phys. Rev. B* **79** 214417
- [34] Tsirlin A A, Schmidt B, Skourski Y, Nath R, Geibel C and Rosner H 2009 *Phys. Rev. B* **80** 132407
- [35] Nath R, Tsirlin A A, Rosner H and Geibel C 2008 *Phys. Rev. B* **78** 064422
- [36] Tsirlin A A, Nath R, Abakumov A M, Shpanchenko R V, Geibel C and Rosner H 2010 *Phys. Rev. B* **81** 174424
- [37] Oba N, Kageyama H, Kitano T, Yasuda J, Baba Y, Nishi M, Hirota K, Narumi Y, Hagiwara M, Kindo K, Saito T, Ajiro Y and Yoshimura K 2006 *J. Phys. Soc. Jpn.* **75** 113601
- [38] Shannon N, Schmidt B, Penc K and Thalmeier P 2004 *Eur. Phys. J. B* **38** 599
- [39] Shannon N, Momoi T and Sindzingre P 2006 *Phys. Rev. Lett.* **96** 027213
- [40] Sindzingre P, Shannon N and Momoi T 2007 *J. Magn. Magn. Mat* **310** 1340
- [41] Schmidt B, Shannon N and Thalmeier P 2007 *J. Phys.: Condens. Matter* **19** 145211
- [42] Schmidt B, Shannon N and Thalmeier P 2007 *J. Magn. Magn. Mater.* **310** 1231
- [43] Viana J R and de Sousa J R 2007 *Phys. Rev. B* **75** 052403
- [44] Sindzingre P, Seabra L, Shannon N and Momoi T 2009 *J. Phys.: Conf. Ser.* **145** 012048
- [45] Sindzingre P, Shannon N and Momoi T 2010 *J. Phys.: Conf. Ser.* **200** 022058
- [46] Härtel M, Richter J, Ihle D and Drechsler S L 2010 *Phys. Rev. B* **81** 174421
- [47] Richter J, Darradi R, Schulenburg J, Farnell D J J and Rosner H 2010 *Phys. Rev. B* **81** 174429
- [48] Nunes W, Viana J R and de Sousa J R 2011 *J. Stat. Mech.* P05016
- [49] Shindou R, Yunoki S and Momoi T 2011 *Phys. Rev. B* **84** 134414
- [50] Momoi T, Sindzingre P and Shannon N 2006 *Phys. Rev. Lett* **97** 257204
- [51] Li P H Y, Bishop R F, Farnell D J J, Richter J and Campbell C E 2012 *Phys. Rev. B* **85** 085115
- [52] Weihong Z, Oitmaa J and Hamer C J 1991 *Phys. Rev. B* **43** 8321
- [53] Beard B B and Wiese U J 1996 *Phys. Rev. Lett.* **77** 5130–5133
- [54] Sandvik A W 1997 *Phys. Rev. B* **56** 11678
- [55] Sandvik A W and Evertz H G 2010 *Phys. Rev. B* **82** 024407

- [56] Farnell D J J, Götze O, Richter J, Bishop R F and Li P H Y 2014 *Phys. Rev. B* **89** 184407
- [57] Villain J 1977 *J. Phys. (France)* **38** 385
- [58] Villain J, Bidaux R, Carton J P and Conte R 1980 *J. Phys. (France)* **41** 1263
- [59] Bishop R F and Kümmel H G 1987 *Phys. Today* **40(3)** 52
- [60] Bartlett R J 1989 *J. Phys. Chem.* **93** 1697
- [61] Arponen J S and Bishop R F 1991 *Ann. Phys. (N.Y.)* **207** 171
- [62] Bishop R F, Parkinson J B and Xian Y 1991 *Phys. Rev. B* **44** 9425
- [63] Bishop R F 1991 *Theor. Chim. Acta* **80** 95
- [64] Bishop R F 1998 *Microscopic Quantum Many-Body Theories and Their Applications* Lecture Notes in Physics Vol. 510 ed Navarro J and Polls A (Berlin: Springer-Verlag) p 1
- [65] Farnell D J J and Bishop R F 2004 *Quantum Magnetism* Lecture Notes in Physics Vol. 645 ed Schollwöck U, Richter J, Farnell D J J and Bishop R F (Berlin: Springer-Verlag) p 307
- [66] Roger M and Hetherington J H 1990 *Phys. Rev. B* **41** 200
- [67] Zeng C, Farnell D J J and Bishop R F 1998 *J. Stat. Phys.* **90** 327
- [68] Krüger S E, Darradi R, Richter J and Farnell D J J 2006 *Phys. Rev. B* **73** 094404
- [69] Darradi R, Derzhko O, Zinke R, Schulenburg J, Krüger S E and Richter J 2008 *Phys. Rev. B* **78** 214415
- [70] Bishop R F, Li P H Y, Farnell D J J and Campbell C E 2009 *Phys. Rev. B* **79** 174405
- [71] Götze O, Farnell D J J, Bishop R F, Li P H Y and Richter J 2011 *Phys. Rev. B* **84** 224428
- [72] Bishop R F, Li P H Y and Campbell C E 2013 *Phys. Rev. B* **88** 214418
- [73] Richter J, Zinke R and Farnell D J J 2015 *Eur. Phys. J. B* **88** 2
- [74] We use the program package CCCM of D. J. J. Farnell and J. Schulenburg, see <http://www-e.uni-magdeburg.de/jschulen/ccm/index.html>
- [75] Farnell D J J and Bishop R F 2008 *Int. J. Mod. Phys. B* **22** 3369
- [76] Bethe H 1931 *Z. Phys.* **71** 205
- [77] Hulthén L 1938 *Ark. Mat. Astron. Fys. A* **26(11)** 1
- [78] Farnell D J J, Bishop R F, Li P H Y, Richter J and Campbell C E 2011 *Phys. Rev. B* **84** 012403
- [79] Li P H Y, Bishop R F and Campbell C E 2013 *Phys. Rev. B* **88** 144423
- [80] Bishop R F and Li P H Y 2012 *Phys. Rev. B* **85** 155135
- [81] Feldner H, Cabra D C and Rossini G L 2011 *Phys. Rev. B* **84** 214406
- [82] Kecke L, Momoi T and Furusaki A 2007 *Phys. Rev. B* **76** 060407(R)
- [83] Sudan J, Lüscher A and Läuchli A M 2009 *Phys. Rev. B* **80** 140402(R)
- [84] Nishimoto S, Drechsler S L, Kuzian R O, van den Brink J, Richter J, Lorenz W E A, Skourski Y, Klingeler R and Büchner B 2011 *Phys. Rev. Lett* **107** 097201

